Thin Solid Films 605 (2016) 108–115

Contents lists available at ScienceDirect

Thin Solid Films

journal homepage: www.elsevier.com/locate/tsf

Low temperature-pyrosol-deposition of aluminum-doped zinc oxide thin films for transparent conducting contacts

M.J. Rivera [a], E.B. Ramírez [b], B. Juárez [a], J. González [a], J.M. García-León [a], L. Escobar-Alarcón [c], J.C. Alonso [a,*]

[a] Instituto de Investigaciones en Materiales, Universidad Nacional Autónoma de México, Apartado Postal 70-360, Coyoacán, 04510 México, D.F., Mexico
[b] Universidad Autónoma de la Ciudad de México, Calle Prolongación San Isidro Núm. 151, Col. San Lorenzo Tezonco, Iztapalapa, 09790 México, D.F., Mexico
[c] Departamento de Física, Instituto Nacional de Investigaciones Nucleares, Apdo. Postal 18-1027, México, D.F. 11801, Mexico

ARTICLE INFO

Article history:
Received 30 April 2015
Received in revised form 18 November 2015
Accepted 20 November 2015
Available online 22 November 2015

Keywords:
ZnO:Al
Thin films
TCO
Ultrasonic spray
Low-temperature pyrolysis
Electrical and optical properties

ABSTRACT

Aluminum doped-zinc oxide (ZnO:Al) thin films with thickness ~1000 nm have been deposited by the ultrasonic spray pyrolysis technique using low substrate temperatures in the range from 285 to 360 °C. The electrical and optical properties of the ZnO:Al (AZO) films were investigated by Uv–vis spectroscopy and Hall effect measurements. The crystallinity and morphology of the films were analyzed using X-ray diffraction (XRD), atomic force microscopy (AFM), and high resolution scanning electron microcopy (SEM). XRD results reveal that all the films are nanocrystalline with a hexagonal wurtzite structure with a preferential orientation in the (002) plane. The size of the grains calculated from Scherrer's formula was in the range from 28 to 35 nm. AFM and SEM analysis reveals that the grains form round and hexagonal shaped aggregates at high deposition temperatures and larger rice shaped aggregates at low temperatures. All the films have a high optical transparency (~82%). According to the Hall measurements the AZO films deposited at 360 and 340 °C had resistivities of 2.2×10^{-3}–4.3×10^{-3} Ω cm, respectively. These films were n-type and had carrier concentrations and mobilities of 3.71–2.54×10^{20} cm^{-3} and 7.4–5.7 cm^2/V s, respectively. The figure of merit of these films as transparent conductors was in the range of 2.6×10^{-2} Ω^{-1}–4.1×10^{-2} Ω^{-1}. Films deposited at 300 °C and 285 °C, had much higher resistivities. Based on the thermogravimetric analysis of the individual precursors used for film deposition, we speculate on possible film growing mechanisms that can explain the composition and electrical properties of films deposited under the two different ranges of temperatures.

© 2015 Elsevier B.V. All rights reserved.

1. Introduction

Due to its abundance, low cost and good chemical stability, compared to indium tin oxide or SnO_2, aluminum doped-zinc oxide (ZnO:Al) thin films, have attracted much attention as transparent conductive contacts for applications in solar cells, electroluminescent displays, organic light emitting devices and other optoelectronic devices [1–6]. A variety of deposition techniques, such as sputtering [1,5–8], pulsed laser deposition [9,10], spin coating [2,11], sol–gel [12–14], pneumatic spray pyrolysis [15–20] and ultrasonic spray pyrolysis (USP) [21–28], have been used for obtaining ZnO:Al (AZO) films with low electrical resistivity and high optical transparency, on different substrates and at different temperatures. For applications of these films as transparent conductive oxides in flexible displays, flexible solar cells, flexible organic light-emitting diodes and other flexible optoelectronic devices that use plastic substrates, low deposition temperatures (≤360 °C) are required [29–32]. The sputtering and pulsed laser deposition techniques allow deposition of AZO films with good optical and electrical properties at low substrate temperatures [5,6,10,30,32]. However these techniques are expensive due to vacuum equipment requirements. The sol gel, spin coating and spray pyrolysis techniques, are much cheaper because in general they do not need vacuum systems, however these techniques usually require of high deposition or annealing temperatures. For example, in the case of spin coating and sol–gel techniques, the preparation of the AZO films takes long times and it requires of multiple processes of coating, drying and annealing at high temperatures (400–550 °C) [2,11–14].

In the case of the spray pyrolysis technique, due to its inherent nature, the substrate temperature must be high enough to decompose the chemical precursors, and the deposition rate is limited to obtain a chemical vapor deposition process on the substrate surface which guarantees the best coating properties. For AZO films deposited using the most common zinc precursors of zinc acetate dihydrate [$Zn(CH_3CO_2)_2 + 2H_2O$], or zinc (II) pentanedionate [$Zn(C_5H_7O_2)_2$], and different Al precursors such as aluminum chloride hexahydrated [$AlCl_3 + 6H_2O$], aluminum (III) pentanedionate [$Al(C_5H_7O_2)_3$], dissolved in different solvents (methanol, ethanol, isopropanol, water), the substrate temperatures to obtain films with low resistivity (~10^{-2}–10^{-3} Ω cm) and high optical transmittance (~85%), are usually in the range of 400–500 °C, for both pneumatic spray pyrolysis [15–18] and ultrasonic [21–28] spray pyrolysis. AZO films with resistivities

* Corresponding author.
E-mail address: alonso@unam.mx (J.C. Alonso).

http://dx.doi.org/10.1016/j.tsf.2015.11.053
0040-6090/© 2015 Elsevier B.V. All rights reserved.

about 3×10^{-3} Ω cm and high transmission ($T \sim 85\%$), have been deposited by pneumatic spray pyrolysis at lower temperatures (380 °C), using a solution of 0.1 M of zinc acetate and 3 at.% of aluminum chloride in a mixture of propanol and de-ionized water in a volumetric proportion of 3:1 [20]. However, the deposition rate of films with these characteristics is relatively low since they require a spray time of 3600 s. AZO films have also been prepared by ultrasonic spray pyrolysis at substrate temperatures of 350 °C, using 0.1 M of zinc acetate dihydrate and 3 at.% of aluminum chloride dissolved in a mixture of absolute methanol, 6-methoxyethanol, some drops of NaOH solution, and stirring and heating at 50 °C for 2 h to yield a clear and transparent solution [21,22]. In this case, highly transparent ($T \sim 80$–90%) AZO films with electrical resistivity about 6.5×10^{-2} Ω cm were obtained.

The purpose of this work was to deposit transparent conducting films of Al-doped ZnO thin films by ultrasonic spray pyrolysis, in a range of relatively low substrate temperatures (285 to 360 °C), using zinc acetate dihydrate and aluminum acetylacetonate as the zinc and aluminum precursors, respectively. The films were deposited on glass substrates, and their structure, morphology, electric resistivity and optical transmittance were investigated.

2. Experimental details

The AZO films were deposited by the ultrasonic spray pyrolysis technique at atmospheric pressure, using a home-made spray system. The start solution was made with 0.2 M of zinc acetate dihydrate [$Zn(CH_3COO)_2 + 2H_2O$] plus 3 at.% of aluminum acetylacetonate [$Al(C_5H_7O_2)_3$] diluted in 8.7 parts of anhydrous methanol, 1 part of deionized water and 0.3 parts of acetic acid. The precursor solution was mixed at room temperature for 10 min with a magnetic stirrer, although it becomes clear and transparent when the acetic acid is added. The substrates were 2.5×2.5 cm^2 corning glass slices, and were cleaned before film deposition, using an ultrasonic bath, first with trichloroethylene, then with acetone and finally with methanol. The films were deposited at atmospheric pressure onto glass substrates heated on a tin bath. Since in the spray deposition system there is an extreme gradient of temperature in the vicinity of the substrate [33], the substrate temperature was measured by contacting a thermocouple at the substrate surface facing the spray. The controller was calibrated with the temperature of the tin bath, in order to get the reported substrate temperatures in the range from 285 to 360 °C. We used high purity dry nitrogen as carrier and director gas at fixed flow rates of 5.2 l/min and 0.65 l/min, respectively. For the deposition of each film, we used the same volume (15 ml) of the starting solution, and this volume was consumed in around 13 min for all depositions. With these deposition parameters, film thickness varied in the range from ~1100 to 1400 nm (see Table 1). The optical transmittance of the films was measured, in the range from 190 to 1100 nm, using a double beam PerkinElmer 35 UV–vis spectrophotometer. The thickness (d_i) of the films deposited was calculated from the interference fringes observed in the optical transmission spectra, using the formula [34]: $d_i = \frac{\lambda_1 \lambda_2}{2n(\lambda_2 - \lambda_1)}$, where λ_1 and λ_2 are the wavelengths of consecutive peaks in the interference pattern, and n is the refractive index of the films. The refractive index of films deposited under the same conditions but with thickness ~100 nm deposited onto silicon substrates (n-type, (100), one side polished) was measured by ellipsometry with a Gaertner 117 ellipsometer using the 632 line from a He–Ne laser. For the calculation of the thickness of the films with the interference fringe formula, we used the measured refractive index for each sample, and peaks λ_1 and λ_2 only in the range from 400 to 850 nm. The thickness (d_p) of the films deposited on glass was also measured with a Sloan Dektac II profilometer. The crystalline structure of the films was determined by X-ray diffraction (XRD) measurements using a Bragg–Brentano Rigaku ULTIMA IV diffractometer with an X-ray source of Cu K_α line (0.15406 nm), at an incidence angle of 1° (grazing beam configuration). The program used to refine and validate the obtained experimental XRD patterns was DIFFRAC PLUS 2005. The surface morphology of the AZO films was investigated by atomic force microscopy (AFM) and scanning electron microscopy (SEM), using a JEOL JSPM-4210 scanning probe microscope and a JEOL 7600F field emission scanning electron microscope (FESEM), respectively. The chemical composition of the films was analyzed by energy dispersive X-ray spectroscopy (EDX) using an EDX INCA X-act by OXFORD spectrometer coupled to the SEM equipment. The operating voltage was 10 kV for the FESEM images. EDX major operating parameters were: working current 4.5×10^{-10} A, voltage 10 kV, working distance 8 mm, and the atomic number-absorption-fluorescence method was used for quantitative analysis.

In order to get a more accurate quantification of the amount of Al incorporated in the films, X-ray photoelectron spectroscopy (XPS) measurements were performed using a K-Alpha Thermo Scientific spectrometer, employing a hemispherical analyzer. The pass energy was kept at 25 eV for narrow scans around the signal of the Al 2p core level, and the scanning step was 0.05 eV. The Al 2p core level spectra were recorded as the average of 100 accumulations in order to improve the signal to noise ratio. The incident radiation was the monochromated radiation of Al-Kα-X-ray (1486.68 eV), with the source working at 12 kV and 6 mA. Argon ion beam etching was performed using a high-flux, low-energy ion source operating at 1500 eV during 60 s.

The electrical resistivity, carrier concentration and mobility of the films were measured at room temperature through Hall measurements by the four point van der Pauw method, using an Ecopia HMS-3000 system. In order to get some insight on the deposition process of the films, we made thermogravimetric-differential thermal analysis (TG-DTG) of the Zn and Al film precursor powders, using a TGA Q5000 V.3.15 equipment from TA Instruments.

3. Results and discussion

3.1. Structure and composition

Fig. 1 shows the XRD patterns for a series of films deposited at different substrate temperatures from 285 to 360 °C. According to the card number 01-070-2551 from PDF-2-(2004) data base the deposited films are polycrystalline, and all of them show a main diffraction peak located at $2\theta = 34.5°$, indicating a growth with a preferential orientation in the (002) plane (the c-axis perpendicular to the substrate surface) of the hexagonal wurtzite ZnO structure, similar to that obtained in AZO films deposited by USP using appropriate precursors, solvents, optimal Al doping level, substrate temperature, etc. [22,25–28,35,36]. The XRD pattern of the film deposited at 285 °C, besides showing the peak corresponding to the (002) plane, shows other peaks at $2\theta = 31.8°$ and

Table 1
Refractive index, thickness measured from optical interference fringes and profilometry, average thickness and band gap energy of AZO films deposited by ultrasonic spray pyrolysis at different substrate temperatures.

Sample	T (°C)	n Refractive index	d_i (nm) (Interference fringe)	d_p (nm) (Prolimetry)	d (nm) (Average thickness)	E_g (eV) (Band gap)
A	360	1.95	1198	1054	1126	3.28
B	340	1.95	1473	1326	1399	3.30
C	320	1.94	1343	1303	1323	3.41
D	300	1.91	1119	1231	1175	3.41
E	285	1.91	1347	1455	1401	3.41

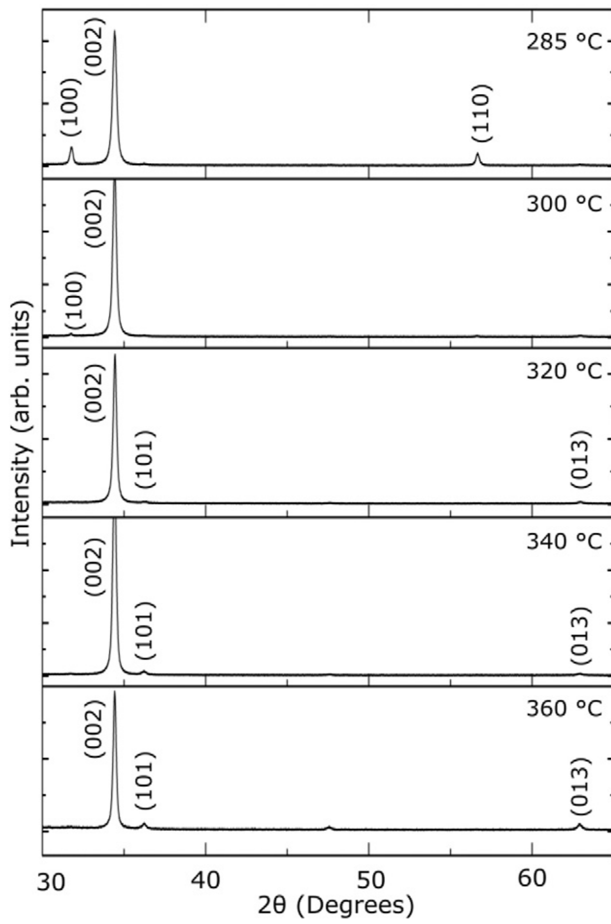

Fig. 1. XRD pattern for aluminum-doped ZnO films as a function of substrate temperature from 285 to 360 °C.

56.6° which correspond to the (100) and (110) orientations of the same wurtzite ZnO structure, respectively. The decrease in the degree of preferred (002) orientation when deposition conditions start to move away from the optimal conditions is in good agreement with other reports [22,25–28,35,36]. The average crystallite size (D) of each film was assessed using the Debye–Scherrer formula:

$$D = \frac{K\lambda}{\beta \cos\theta}$$

Table 2
Composition, thickness, grain size, electrical and electronic properties of AZO films deposited by ultrasonic spray pyrolysis at different substrate temperatures.

Sample	EDX (at.%)	d (nm)	D (nm)	ρ (Ohm-cm)	R_s (Ohm/□)	n_e (cm^{-3})	μ (cm^2/V s)
A	Zn: 49.2 O: 50.8 Al: –	1126	34.9	2.23×10^{-3}	19.8	3.71×10^{20}	7.46
B	Zn: 50.3 O: 49.7 Al: –	1399	32.6	4.3×10^{-3}	30.7	2.54×10^{20}	5.7
C	Zn: 49.2 O: 50.8 Al: –	1323	33	1.38×10^{-2}	104.3	1.89×10^{20}	2.36
D	Zn: 48.2 O: 50.0 Al: 0.8	1175	30.5	2.95×10^{-1}	25×10^2	3.05×10^{18}	6.8
E	Zn: 48.8 O: 50.3 Al: 0.9	1401	27.7	5.55	39×10^3	5.46×10^{16}	20.46

where, λ is the X-ray wavelength (0.15406 nm), β is the full width at half maximum of the (002) peak, θ is the Bragg diffraction angle of this peak, and K is the correction factor (0.9).

As Table 2 shows, the grain sizes were in the range from 27 nm to 35 nm, and the size shows the trend to have a small increase by increasing the substrate temperature.

Fig. 2 depicts the AFM and FESEM micrographs for the AZO films deposited at the highest (sample A) and the lowest (sample E) substrate temperature. From the AFM micrograph of Fig. 2a) we find that the AZO film deposited at 360 °C (sample A) consists of round shaped aggregates (with sizes around 100–125 nm), of grains with sizes around 30–35 nm. In consistency with this AFM image, the FESEM micrograph for the same sample A (Fig. 2b), shows agglomerates of round and hexagonal shaped and well packed agglomerates, with average size around 100 nm. The regular and highly oriented hexagonal columnar structures observed in this figure are in good agreement with the preferential orientation observed in the XRD spectrum of this film, and is consistent with the structures found for other AZO films deposited by USP in optimal conditions [23,24,27]. The AFM and FESEM images of Fig. 2c) and d), show that the AZO film deposited at the lowest substrate temperature of 285 °C (sample E), is also formed of grains aggregates with sizes around or slight smaller than 30 nm, but in this case the agglomerates are larger and stretched or rice shaped, and are less densely packed. Similar structures to that of sample E have been also observed in AZO films deposited by USP in deposition conditions of high Al doping where there are extra-aluminum atoms in the films, which may occupy interstitial position that affect the nucleation and coalescence of islands during the process of film growth, and give rise to elongated agglomerates [27]. The morphology of sample E, is consistent with the morphology reported for other AZO films deposited by USP at low temperatures, which tend to have a non faceted, elongated grains with high aspect ratios [37]. Fig. 3 shows a cross section FESEM micrograph of the AZO film (E) deposited at 285 °C. As can be seen the film appears well adhered to the substrate and the islands on the surface can be clearly seen. From the AFM and FESEM analysis of the other samples we observed that the morphology of samples B and C was closer to that of sample A, meanwhile the morphology of sample D was closer to that of sample E. It must be pointed out that sizes of the grains observed in the AFM images of all the samples, were in the same order than the sizes calculated for the nanocrystallites from the XRD analysis, and with the same tendency to have a small decrease as the substrate temperature was decreased. The elemental compositions of the AZO films, obtained from the EDX spectra are shown in Table 2. Fig. 4a) and b) shows the EDX spectra of samples A and E. According to the compositions shown in Table 2 for the samples A, B and C, which were deposited at substrate temperatures T ≥ 320 °C, the atomic percentages of zinc and oxygen were near the 50 at.% indicating that they are composed of nearly stoichiometric ZnO. The absence of the Al characteristic peaks in the EDX spectra of these samples, as it is absent in the spectrum of sample A of Fig. 4a), indicates that the incorporation of Al atoms in these AZO films is in a very low relative concentration and below the limit of detection of the X-ray spectrometer. This means that samples A, B and C, have aluminum concentrations at a doping level. In contrast, the EDX spectra of sample D and E showed, as in Fig. 4b), a small peak characteristic of Al, and according to Table 2, these samples had [Al]/[Zn] ratios of 1.6% and 1.8%, respectively. XPS measurements of the Al 2p core level peak were made to get more insight on the percentage of Al doping in the films. Fig. 5 shows the Al 2p core level XPS spectra for all the films. As can be seen the intensity of the Al 2p signal increases slightly as the substrate temperature increases, except for the sample B, for which the signal is hindered by the noise. As this figure shows, sample A, deposited at the highest substrate temperature has 0.2% of Al, and the percentage of Al increases up to 1% for the sample E deposited at the lowest temperature. The percentage of Al in samples D and E deposited at low temperature is in good agreement with the percentages obtained by EDX. It is also clear from the XPS spectra that the position of the peak shifts from 73.8 to

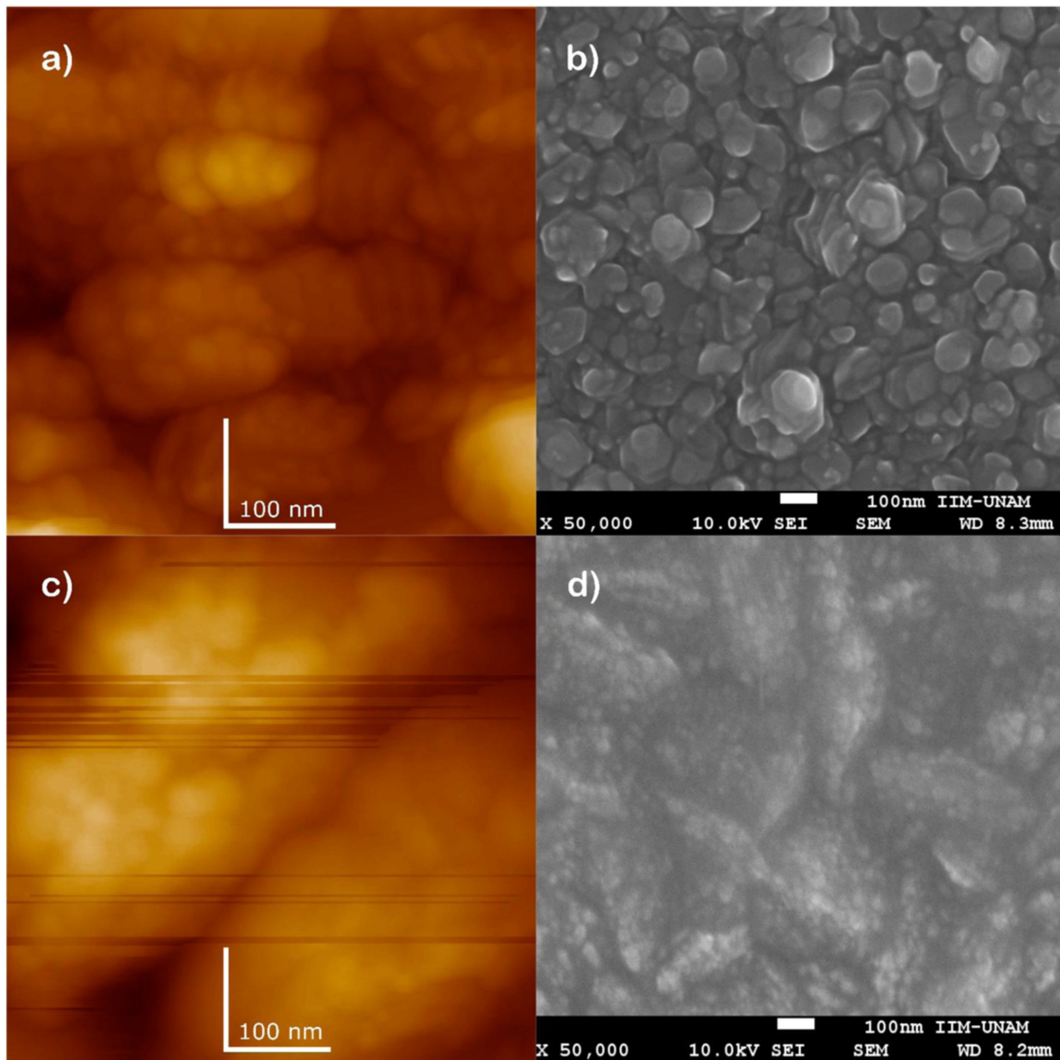

Fig. 2. AFM images and FESEM micrographs for AZO films deposited at the highest and the lowest substrate temperature. AFM images for (a) 360 °C and (c) 285 °C; SEM micrographs for (b) 360 °C and (d) 285 °C.

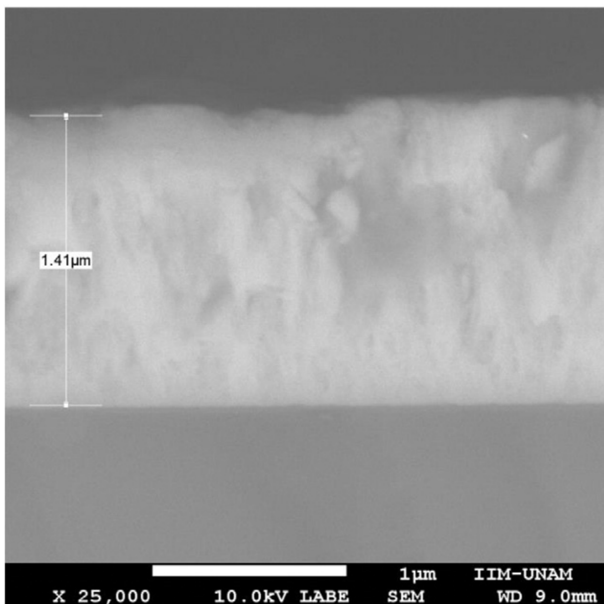

Fig. 3. Cross section FESEM micrograph of aluminum-doped ZnO film deposited at 285 °C.

74.6 eV as the substrate temperature decreases, indicating that the Al atoms tend to form aluminum suboxides, Al_2O_{3-x} [38].

3.2. Optical and electrical properties

The optical transmittance of the AZO films deposited with different substrate temperatures was measured with reference to the air and the resulting transmittance spectra are shown in Fig. 6. It may be seen that all the films are highly transparent over the visible and near infrared regions, independently of deposition temperature. The average transmittance, in the range from 400 to 800 nm, was around 82% for all the samples. The refractive index and thickness of the films are shown in Table 1. Table 1 also shows the band gap of the films which was calculated by taking the plot of $(\alpha h\nu)^2$ *vs* $h\nu$, corresponding to optical absorption by direct transitions [21,39,40], where, $\alpha = -\frac{1}{d}\ln(T)$, is the absorption coefficient, $h\nu$ is the photon energy, T is the transmittance and d is the film thickness. As Table 1 shows the band gap of films A and B deposited at higher temperatures is lower (3.28 and 3.30 eV) than the band gap of the films C, D and E (3.41 eV) deposited at lower temperatures. This increase in the band gap is consistent with the increase in the Al content observed in the films from the XPS measurements [21,26,40]. The increase in the band gap is also consistent with the decrease in the refractive of the films (see Table 1) [40].

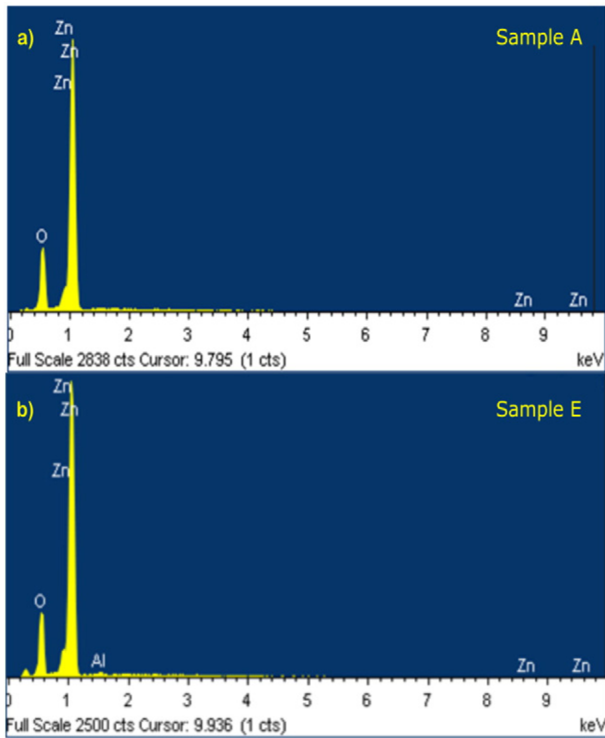

Fig. 4. EDX spectra of AZO films at (a) 360 °C, and (b) 285 °C substrate temperature.

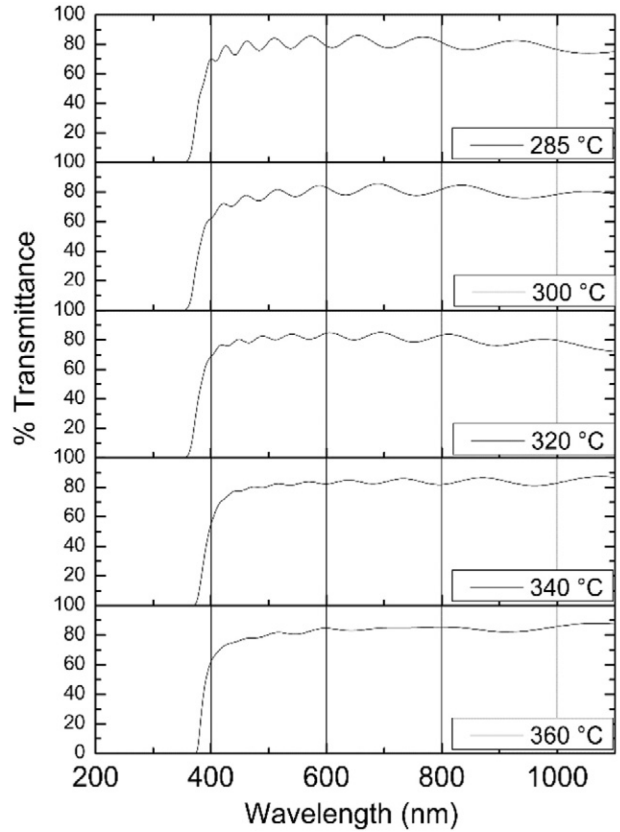

Fig. 6. Optical transmission spectra of aluminum-doped zinc oxide films deposited at different substrate temperatures from 285 °C to 360 °C. It can be observed that for all substrate temperature transmittance is around 82% in average.

The electrical resistivity (ρ), carrier concentration (n_e) and mobility (μ) of the AZO films were evaluated from Hall measurements using the van der Pauw method on samples with square geometry and small contacts located on the periphery. The values of these parameters are listed in Table 2, and according to the negative sign of the obtained Hall coefficient, all the films were n-type.

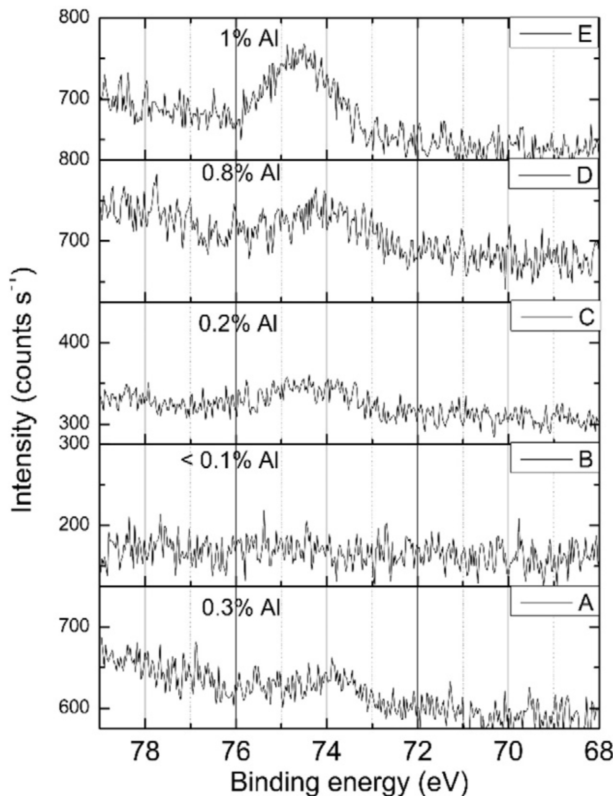

Fig. 5. Aluminum 2p core level XPS spectra for all films. It can be observed a shift to higher energies when the temperature is decreased as indicator of Al_2O_{3-x} formation.

The plot of the electrical resistivity and carrier concentration of the AZO films as a function of substrate temperature is shown in Fig. 7. As can be seen from this figure and Table 2, the lowest resistivity (in the order of 10^{-3} Ω cm) and the highest carrier concentrations (in the order of 10^{20} cm^{-3}) correspond to sample A, which was deposited at the highest temperature (360 °C). Although the resistivity and carrier concentration of sample B deposited at 340 °C is of the same order of magnitude than sample A, these parameters decrease significantly for the samples C, D and E deposited at lower temperatures. As Table 2

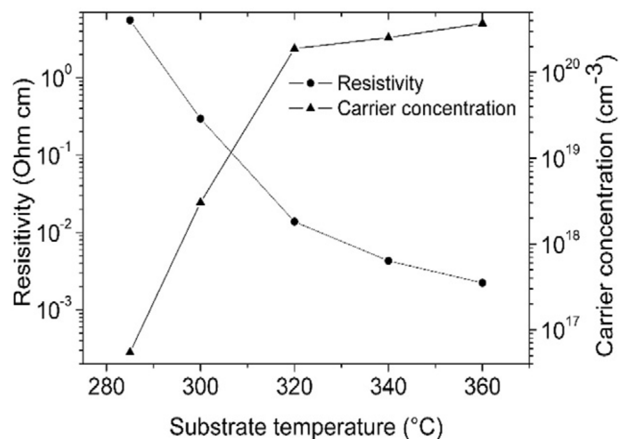

Fig. 7. Electrical resistivity and carrier concentration in AZO films plotted as a function of substrate temperature.

shows the mobility of the films first decreases as the substrate temperature decreases and has a minimum for the film deposited at 320 °C, and then increase for lower substrate temperatures. The decrease in the electrical resistivity as the substrate temperature decreases is a trend generally found in AZO films deposited by both, pneumatic spray pyrolysis and ultrasonic spray pyrolysis [15,24,27]. The increase in the electrical resistivity and mobility of the films as the substrate temperature is decreased can be associated with the decrease in the preferential orientation of the AZO grains and the formation of Al_2O_{3-x} clusters [25]. The increase of the mobility of films D and E deposited at lower temperatures is not well understood at present, but a similar behavior has been already observed in AZO films deposited by USP in a higher range of temperatures [27].

According to the values of the sheet resistances (R_s) of samples A and B shown in Table 2, and their optical transmission ($T \approx 0.82$), the figure of merit as transparent conductors [41], $F_{TC} = T / R_s$, was calculated for these films and they were in the range of $2.6 \times 10^{-2}\ \Omega^{-1}$ and $4.1 \times 10^{-2}\ \Omega^{-1}$.

3.3. Correlation of film growing and film properties

In order to speculate on the possible growing mechanisms of the film, we made thermogravimetric analysis (TGA) of the individual powders of zinc and aluminum precursors, to measure their temperatures of thermal decomposition. Fig. 8a) and b) shows the TGA curves of zinc acetate dihydrate [$Zn(CH_3COO)_2 + 2H_2O$] and aluminum acetylacetonate [$Al(C_5H_7O_2)_3$], respectively, at a heating rate of 5 °C/min in dry nitrogen flow. Based on some previous works on the thermal decomposition of zinc acetate dehydrate [42–44], and the TG-DTG curves of Fig. 8a), we can infer that the first mass loss of the [$Zn(CH_3COO)_2 + 2H_2O$] is the thermal dehydration or loss of the two water molecules, which starts at approximately 70 °C and finish at ~108 °C. The other two steps of mass loss, one starting at ~200 °C and the other starting at ~255 °C and finally reaching the total mass loss of 100% at a final point of 300 °C, indicate the thermal decomposition of the [$Zn(CH_3COO)_2$], with the simultaneous evolution of acetone, carbon dioxide (or other hydrocarbons or oxygenated hydrocarbons, depending on the heating rate) from the acetate groups, and without the formation of ZnO. The TGA curves of Fig. 8b), show that the thermal decomposition of [$Al(C_5H_7O_2)_3$] starts from ~150 °C and it is completed at ~210 °C, without the formation of Al_2O_3. These results are consistent with a previous work [45], where it has been reported that aluminum acetylacetonate begins to decompose at 160 °C and its decomposition is completed at ~220 °C.

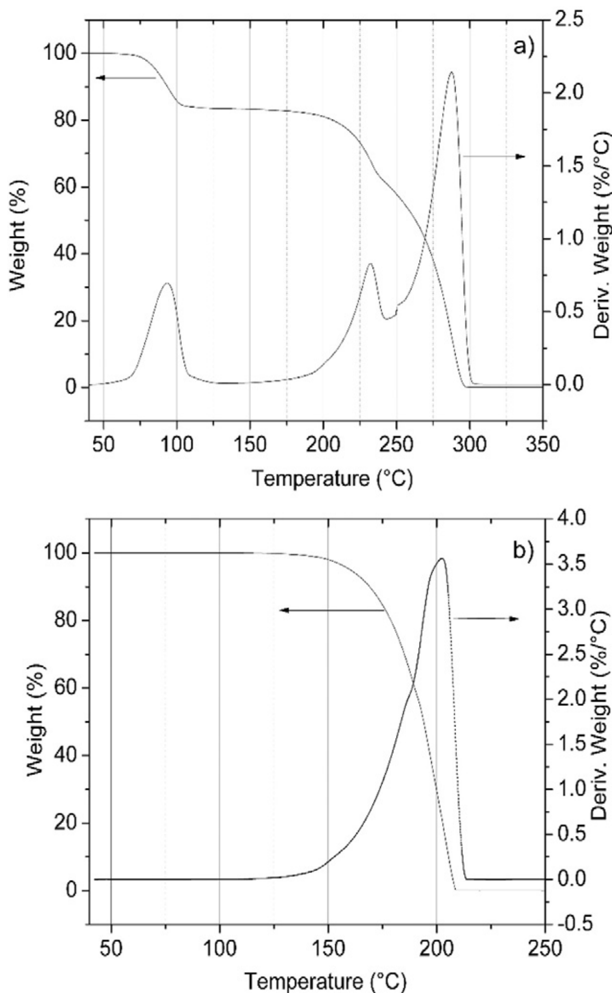

Fig. 8. TG-DTG curves for (a) zinc and (b) aluminum precursors evaluated at 5 °C/min heating rate carried out in a nitrogen gas atmosphere.

In addition to our TGA results which indicate that the [Al(C5H7O2)3] precursor decomposes completely at a lower temperature (~210 °C) than the [$Zn(CH_3COO)_2 + 2H_2O$] precursor (~300 °C), it has been reported that during a dynamic thermal process of zinc acetate [$Zn(CH_3COO)_2$], in a humidity controlled atmosphere, ZnO can be formed following the chemical reaction [42].

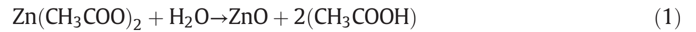

$$Zn(CH_3COO)_2 + H_2O \rightarrow ZnO + 2(CH_3COOH) \quad (1)$$

On the other hand, the decomposition of $Al(C_5H_7O_2)_3$ in flowing air at temperatures in the range from 257 to 300 °C, can result in the formation of very fine particles of Al_2O_3, but at temperatures higher than 300 °C forms other volatile Al-complexes [46].

Based on our TGA analysis and the abovementioned works, and since we used water in our precursor solution (8.7 parts of anhydrous methanol, 1 part of deionized water), we can speculate that for the AZO films named as samples A, B and C, which were deposited at temperatures higher than 300 °C, as the drops of the precursor solution arrive on the substrate surface, the [$Zn(CH_3COO)_2$] molecules are decomposed completely and the pyrolytic reaction (1), which give rise to the formation of the ZnO film occurs efficiently. In parallel with the reaction (1) the 3 at.% of the dopant-aluminum precursor molecules of [$Al(C_5H_7O_2)_3$] can be also completely decomposed, generating Al-complexes, that give rise to the incorporation of a small amount of Al atoms in the growing ZnO film, by substituting Zn atoms. As it is known, if the Al^{3+} ions have the chance to be incorporated in the substitutional sites of the Zn^{2+} cations of the ZnO wurtzite network, the atomic substitution (Al–Zn) adds one extra valence electron into the system, since Al atom possesses three valence electrons whilst Zn atom has only two valence electrons [47]. Consequently, in this case, each Al atom that substitutes a Zn atom generates a free electron in the conduction band of the AZO films. The low content of substitutional Al atoms incorporated (undetectable by EDX and below 1 at.% according to XPS measurements) in the A, and C films, is consistent with the free carrier concentration measured in these films by Hall effect. The concentration of Zn atoms in the ZnO film, can be roughly calculated to be: $n_{Zn} = \frac{N_{Zn}}{V} = \frac{N_A \rho_{Zn}}{(M_{Zn}+M_O)} \approx 4.0 \times 10^{22}\ \text{cm}^{-3}$, assuming $\rho_{Zn} \approx 5.4\ \text{g/cm}^3$ (lower than 5.606 g/cm^3 for bulk ZnO), $M_{Zn} = 65.38$ g, $M_O = 15.999$ g, and N_A is the Avogadro's number. Then, if we assume that the electron concentration, n_e, in these films is equal to the concentration, n_{Al}, of Al atoms that substitute Zn atoms, the percentage of Al atoms incorporated in the films is $\frac{n_{Al}}{n_{Zn}} = \frac{n_e}{n_{Zn}}$. Using the carrier concentration measured for films A and C (see Table 2), the percentages of Al atoms incorporated in these films are in the range of ~0.9–0.45 at.%.

For the films named as samples D and E, which were deposited at substrate temperatures equal or lower than 300 °C, we expect an incomplete thermal decomposition of the [$Zn(CH_3COO)_2$] precursor and/or a low rate of the pyrolytic reactions (1) that form the ZnO

phase. We can also assume that in this case, in parallel with the inefficient formation of the ZnO phase, some of the Al atoms generated by the thermal decomposition of the $[Al(C_5H_7O_2)_3]$, form the alumina phase (Al_2O_3) [25,46], instead of incorporating as n-type dopants by substituting Zn atoms in the ZnO network. This growing model for the films deposited and low temperatures is consistent with the low carrier concentration and high resistivity found for samples D and E, and the fact shown in Table 2, that the decrease in carrier concentration and increase in resistivity seems to be proportional to the content of aluminum incorporated in the film as alumina. The low carrier mobility of sample D and E can be due to the segregation of the Al_2O_3 phase in the grain boundaries. The shift in the Al 2p core peak toward higher energies observed in the XPS spectra of the films deposited at low temperatures is also indicative of the formation Al_2O_{3-x} clusters in these films.

4. Conclusion

In summary, in this investigation an attempt has been made to deposit at low substrate temperatures (285 to 360 °C) by ultrasonic spray pyrolysis, AZO films with good optical and electrical properties for applications as transparent conductive contacts. We have used substrate temperatures close to the temperatures of thermal decomposition of the $[Zn(CH_3COO)_2 + 2H_2O]$ and $[Al(C_5H_7O_2)_3]$ precursors used for film deposition. Our results indicate that for films deposited at substrate temperatures higher than 300 °C, the Al atoms are incorporated in the growing ZnO phase, mainly by substituting Zn atoms and giving rise to n-type doping and low electrical resistivity. On the other hand, films deposited at substrate temperatures equal or lower than 300 °C, result with much higher resistivity in spite that they have a higher Al content. We speculate that the high resistivity of these films is because at low substrate temperatures the $[Zn(CH_3COO)_2 + 2H_2O]$ precursor decomposes incompletely or inefficiently and the Al generated from the $[Al(C_5H_7O_2)_3]$ decomposition forms Al_2O_{3-x} clusters. The optical transparency in the visible range of the AZO films investigated in this work was almost independent of substrate temperatures.

Acknowledgments

The authors want to acknowledge the technical assistance of A. Tejeda, D. Cabrero, C. Flores, O. Novelo, J. Romero-Ibarra, M.A. Canseco and Fernando Silvar of IIM-UNAM. This research work was partially supported under project PAPIIT-UNAM number IG100614-2.

References

[1] R.N. Chauhan, R.S. Anand, J. Kumar, RF-sputtered Al-doped ZnO thin films: optoelectrical properties and application in photovoltaic devices, Phys. Status Solidi 9 (2014) 1–9.
[2] A.A. Al-Ghamdi, O.A. Al-Hartomy, M. El Okr, A.M. Nawar, S. El-Gazzar, F. El-Tantawy, et al., Semiconducting properties of Al doped ZnO thin films, Spectrochim. Acta A Mol. Biomol. Spectrosc. 131 (2014) 512–517.
[3] Y. Ammaih, A. Lfakir, B. Hartiti, A. Ridah, P. Thevenin, M. Siadat, Structural, optical and electrical properties of ZnO:Al thin films for optoelectronic applications, Opt. Quant. Electron. 46 (2013) 229–234.
[4] E.B. Ramírez, M. Bizarro, J.C. Alonso, Synthesis and characterization of thin film electroluminescent devices all-prepared by ultrasonic spray pyrolysis, Thin Solid Films 548 (2013) 255–258.
[5] B.S. Chua, S. Xu, Y.P. Ren, Q.J. Cheng, K. Ostrikov, High-rate, room temperature plasma-enhanced deposition of aluminum-doped zinc oxide nanofilms for solar cell applications, J. Alloys Compd. 485 (2009) 379–384.
[6] J. Zhao, S. Xie, S. Han, Z. Yang, L. Ye, T. Yang, Organic light-emitting diodes with AZO films as electrodes, Synth. Met. 114 (2000) 251–254.
[7] N.E. Duygulu, A.O. Kodolbas, A. Ekerim, Influence of deposition parameters on ZnO and ZnO:Al thin films, Phys. Status Solidi C 11 (2014) 1460–1463.
[8] Y. Kim, W. Lee, D.-R. Jung, J. Kim, S. Nam, H. Kim, et al., Optical and electronic properties of post-annealed ZnO:Al thin films, Appl. Phys. Lett. 96 (2010) 171902.
[9] R. Vinodkumar, I. Navas, S.R. Chalana, K.G. Gopchandran, V. Ganesan, R. Philip, et al., Highly conductive and transparent laser ablated nanostructured Al:ZnO thin films, Appl. Surf. Sci. 257 (2010) 708–716.
[10] X.Q. Gu, L.P. Zhu, L. Cao, Z.Z. Ye, H.P. He, P.K. Chu, Optical and electrical properties of ZnO:Al thin films synthesized by low-pressure pulsed laser deposition, Mater. Sci. Semicond. Process. 14 (2011) 48–51.
[11] S.P. Shrestha, R. Ghimire, J.J. Nakarmi, Y.-S. Kim, S. Shrestha, C.-Y. Park, et al., Properties of ZnO:Al films prepared by spin coating of aged precursor solution, Bull. Kor. Chem. Soc. 31 (2010) 112–115.
[12] S. Mridha, D. Basak, Aluminium doped ZnO films: electrical, optical and photoresponse studies, J. Phys. D. Appl. Phys. 40 (2007) 6902–6907.
[13] I.Y.Y. Bu, Sol–gel production of aluminium doped zinc oxide using aluminium nitrate, Mater. Sci. Semicond. Process. 27 (2014) 19–25.
[14] M. Alhamed, W. Abdullah, Structural and optical properties of ZnO:Al films prepared by the sol–gel method, J. Electron. Devices 7 (2010) 246–252.
[15] S.M. Rozati, S. Akesteh, Characterization of ZnO:Al thin films obtained by spray pyrolysis technique, Mater. Charact. 58 (2007) 319–322.
[16] S.M. Rozati, Effect of film thickness on the physical properties of ZnO:Al thin films deposited using a spray pyrolysis technique, Can. J. Phys. 86 (2008) 379–382.
[17] H. Mondragon, A. Maldonado, M. Olvera, A. Reyes, R. Castanedo, G. Torres, et al., ZnO :Al thin films obtained by chemical spray : effect of the Al concentration, Appl. Surf. Sci. 193 (2002) 52–59.
[18] L. Castañeda, R. Silva-González, J.M. Gracia-Jiménez, M.E. Hernández-Torres, M. Avendaño-Alejo, C. Márquez-Beltrán, et al., Influence of aluminum concentration and substrate temperature on the physical characteristics of chemically sprayed ZnO:Al thin solid films deposited from zinc pentanedionate and aluminum pentanedionate, Mater. Sci. Semicond. Process. 13 (2010) 80–85.
[19] S.J. Ikhmayies, N.M. Abu El-Haija, R.N. Ahmad-Bitar, Electrical and optical properties of ZnO:Al thin films prepared by the spray pyrolysis technique, Phys. Scr. 81 (2010) 015703.
[20] Z. Ben Achour, T. Ktari, B. Ouertani, O. Touayar, B. Bessais, J. Ben Brahim, Effect of doping level and spray time on zinc oxide thin films produced by spray pyrolysis for transparent electrodes applications, Sensors Actuators A Phys. 134 (2007) 447–451.
[21] A. Gahtar, A. Rahal, B. Benhaoua, S. Benramache, A comparative study on structural and optical properties of ZnO and Al-doped ZnO thin films obtained by ultrasonic spray method using different solvents, Opt. - Int. J. Light Electron Opt. 125 (2014) 3674–3678.
[22] A.A. Gahtar, S. Benramache, B. Benhaoua, F. Chabane, Preparation of transparent conducting ZnO:Al films on glass substrates by ultrasonic spray technique, J. Semicond. 34 (2013) 073002.
[23] G. Kenanakis, N. Katsarakis, Ultrasonic spray pyrolysis growth of ZnO and ZnO:Al nanostructured films: application to photocatalysis, Mater. Res. Bull. 60 (2014) 752–759.
[24] E. Arca, K. Fleischer, I. Shvets, Tuning the crystallographic, morphological, optical and electrical properties of ZnO:Al grown by spray pyrolysis, Thin Solid Films 555 (2014) 9–12.
[25] L. Dong, T.F. Pei, H.Q. Li, D.Y. Xu, Deposition of ZnO:Al thin films by ultrasonic spray pyrolysis, Adv. Mater. Res. 150-151 (2010) 1617–1620, http://dx.doi.org/10.4028/www.scientific.net/AMR.150-151.1617.
[26] R. Pandey, S. Yuldashev, H.D. Nguyen, H.C. Jeon, T.W. Kang, Fabrication of aluminium doped zinc oxide (AZO) transparent conductive oxide by ultrasonic spray pyrolysis, Curr. Appl. Phys. 12 (2012) S56–S58.
[27] B.J. Babu, A. Maldonado, S. Velumani, R. Asomoza, Electrical and optical properties of ultrasonically sprayed Al-doped zinc oxide thin films, Mater. Sci. Eng. B 174 (2010) 31–37.
[28] J.-H. Lee, B.-O. Park, Characteristics of Al-doped ZnO thin films obtained by ultrasonic spray pyrolysis: effects of Al doping and an annealing treatment, Mater. Sci. Eng. B 106 (2004) 242–245.
[29] MacDonald, Engineered films for display technologies, J. Mater. Chem. 14 (2004) 4–10.
[30] S. Fernández, F.B. Naranjo, Optimization of aluminum-doped zinc oxide films deposited at low temperature by radio-frequency sputtering on flexible substrates for solar cell applications, Sol. Energy Mater. Sol. Cells 94 (2010) 157–163.
[31] C. Guillén, J. Herrero, TCO/metal/TCO structures for energy and flexible electronics, Thin Solid Films 520 (2011) 1–17.
[32] G. Socol, M. Socol, N. Stefan, E. Axente, G. Popescu-Pelin, D. Craciun, et al., Pulsed laser deposition of transparent conductive oxide thin films on flexible substrates, Appl. Surf. Sci. 260 (2012) 42–46.
[33] J.C. Vigui, J. Spitz, Chemical vapor deposition at low temperatures, J. Electrochem. Soc. 122 (1975) 585–588.
[34] A.M. Goodman, Optical interference method for the approximate determination of refractive index and thickness of a transparent layer, Appl. Opt. 17 (1978) 2779–2787.
[35] G. Kenanakis, N. Katsarakis, E. Koudoumas, Influence of precursor type, deposition time and doping concentration on the morphological, electrical and optical properties of ZnO and ZnO:Al thin films grown by ultrasonic spray pyrolysis, Thin Solid Films 555 (2014) 62–67.
[36] B.J. Babu, A. Maldonado, S. Velumani, Deposition and characterization of ZnO:Al thin films by ultrasonic spray pyrolysis, 2009 6th Int. Conf. Electr. Eng. Comput. Sci. Autom. Control 2009, pp. 1–5.
[37] J. Xu, H. Wang, L. Yang, M. Jiang, S. Wei, T. Zhang, Low temperature growth of highly crystallized ZnO:Al films by ultrasonic spray pyrolysis from acetylacetone salt, Mater. Sci. Eng. B 167 (2010) 182–186.
[38] N. Reddy, P. Bera, V.R. Reddy, N. Sridhara, A. Dey, C. Anandan, et al., XPS study of sputtered alumina thin films, Ceram. Int. 40 (2014) 11099–11107.
[39] M. Krunks, E. Mellikov, Zinc oxide thin films by the spray pyrolysis method, Thin Solid Films 270 (1995) 33–36.
[40] H. Benzarouk, A. Drici, M. Mekhnache, A. Amara, M. Guerioune, J.C. Bernède, et al., Effect of different dopant elements (Al, Mg and Ni) on microstructural, optical and electrochemical properties of ZnO thin films deposited by spray pyrolysis (SP), Superlattice. Microst. 52 (2012) 594–604.

[41] G. Haacke, New figure of merit for transparent conductors, J. Appl. Phys. 47 (1976) 4086–4089.
[42] T. Arii, A. Kishi, The effect of humidity on thermal process of zinc acetate, Thermochim. Acta 400 (2003) 175–185.
[43] A.V. Ghule, K. Ghule, C.-Y. Chen, W.-Y. Chen, S.-H. Tzing, H. Chang, et al., In situ thermo-TOF-SIMS study of thermal decomposition of zinc acetate dihydrate, J. Mass Spectrom. 39 (2004) 1202–1208.
[44] A. Vithal Ghule, B. Lo, S.-H. Tzing, K. Ghule, H. Chang, Y. Chien Ling, Simultaneous thermogravimetric analysis and in situ thermo-Raman spectroscopic investigation of thermal decomposition of zinc acetate dihydrate forming zinc oxide nanoparticles, Chem. Phys. Lett. 381 (2003) 262–270.
[45] Y.H. Hwang, J.H. Jeon, S.-J. Seo, B.-S. Bae, Solution-processed, high performance aluminum indium oxide thin-film transistors fabricated at low temperature, Electrochem. Solid-State Lett. 12 (2009) H336–H339.
[46] M. Shirodker, V. Borker, C. Nather, W. Bensch, K.S. Rane, Synthesis and structure of tris (acetylacetonato) aluminum (III), Indian J. Chem. 49 (2010) 1607–1611.
[47] F. Maldonado, A. Stashans, Al-doped ZnO: electronic, electrical and structural properties, J. Phys. Chem. Solids 71 (2010) 784–787.